

## Magneto-optics of electronic transport in nanowires

S. Blom, L. Y. Gorelik, M. Jonson, and R. I. Shekhter

*Department of Applied Physics, Chalmers University of Technology and Göteborg University, S-412 96 Göteborg, Sweden*

A. G. Scherbakov, E. N. Bogachek, and Uzi Landman

*School of Physics, Georgia Institute of Technology, Atlanta, Georgia 30332-0430*

(Received 9 July 1998)

Effects of irradiation on the electronic conductance in nanowires, for field-free conditions and under the influence of applied longitudinal magnetic fields, were investigated. The nanowires were modeled within the free-electron framework with a parabolic (transverse) confining potential. Our results for the dependence of the photoconductance of irradiated nanowires on the photon energy and/or the strength of the applied magnetic field show that such measurements may be used as a magneto-optic spectroscopy for determination of (i) the electron Fermi energy, (ii) the electron effective mass, and (iii) the number of quantized modes in the nanowire. Such measurements may also be used to assess to what degree the electron transport through the nanowire is adiabatic. Furthermore, our results suggest a method for controlling and tuning electronic transport in nanowires via external electromagnetic fields. [S0163-1829(98)07348-2]

### I. INTRODUCTION

Materials structures with spatial dimensions reduced to the nanometer-scale regime often exhibit unique structural, electronic, spectral, transport, and mechanical properties, which cannot be extrapolated from behavior at larger sizes, making them objects of significant fundamental and technological interest. Early predictions pertaining to formation mechanisms, energetics, mechanical response, and structural evolution of three-dimensional (3D) crystalline nanowires generated upon elongation of a contact between material bodies<sup>1,2</sup> led to intensive theoretical and experimental investigations of such systems.<sup>2,3</sup> Measurements corroborated the early theoretical predictions, through studies of mechanical, structural, and transport properties in nanowires formed through contact elongation, using tip-based methods, controllable break junctions, and pin-plate techniques.<sup>3</sup> Focusing our discussion on electronic transport, it has been found, as anticipated,<sup>1,4</sup> that indeed such nanowires can be used to study quantum effects on the conductance in 3D narrow constrictions, via exhibiting room-temperature conductance quantization (in units of the conductance quantum  $2e^2/h$ ), in analogy with conductance quantization found under cryogenic conditions in two-dimensional electron gases (2DEG) in semiconductor heterostructures controlled by electrostatic gates.<sup>5</sup>

As in the 2DEG case, it is convenient to analyze the quantum transport of electrons in 3D nanowires in the framework of the adiabatic approximation; that is, when the variation of the nanowire's shape (along its longitudinal axis) occurs on a scale larger than the electron Fermi wavelength  $\lambda_F$ , resulting in no mode mixing between the conducting channels.<sup>6</sup> In order to investigate the nature of electronic transport in 3D nanowires, as well as to assess the validity of the adiabatic transport mode, it is of special importance to probe the electronic quantum states and transport characteristics in such systems in a controllable manner. This is a particularly difficult task, since using current methods both the electronic

spectrum and (atomic, or crystalline) structure of the nanowire are influenced in the process of mechanical elongation.<sup>1-3,7</sup> To this aim, methods for controlling and tuning the conductance in such systems, for a given nanowire configuration, through the use of external fields (without influencing the geometric structure of the wire) have been investigated, including magnetic fields<sup>8</sup> and finite voltages (in conjunction with magnetic fields<sup>9(a)</sup> or under field-free conditions<sup>9(a),9(b)</sup>).

In the present paper we suggest the use of microwave irradiation for spectroscopy of quantum electronic states and transport in nanowires.<sup>10</sup> We show that the use of irradiation in conjunction with an applied (static) magnetic field may provide a tool for investigations of the following electronic and transport properties of nanowires: (i) adiabaticity of the electronic transport, (ii) the value of the Fermi energy of electrons in the nanowire, (iii) the value of the electronic effective mass, and (iv) the number of quantized electronic modes in the nanowire. Issues (ii) and (iii) are of special importance because, due to band bending and strong structural and mechanical deformations of the material in the nanowire, these parameters could be different from those in the bulk. Point (iv) may serve as an additional tool to estimate the cross-sectional sizes of metallic nanoconstrictions.

The main advantage of the use of microwave irradiation in investigations of nanowires originates from the strong sensitivity of the nature of electronic transport on the adiabaticity of the electronic propagation in the wire. Electromagnetic irradiation cannot typically affect transport properties of bulk metals because the momentum transfer caused by electron-photon scattering events is very small. The situation is different in nanowires where, due to the reduced dimensions, electronic states transverse to the axis of the wire direction are quantized. In this case photon-assisted transitions between such quantized states become possible. It is particularly important that in the case of adiabatic propagation such optical transitions strongly affect the electronic transport in the longitudinal direction.<sup>11-13</sup> This follows from the fact

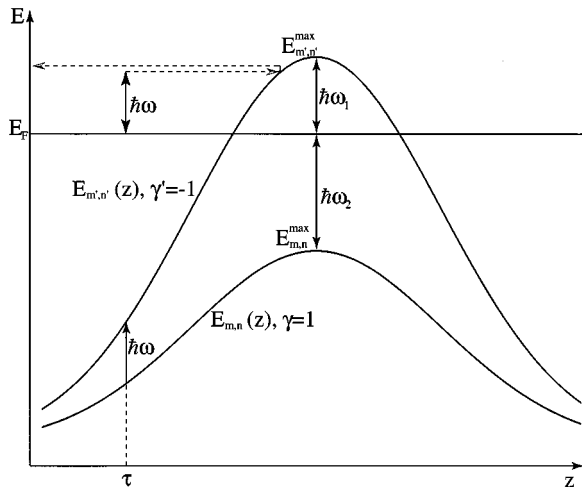


FIG. 1. Effective 1D potential barriers for the longitudinal propagation of an electron at the Fermi level, occupying the transverse state  $(m, n)$ . A photoinduced transition is shown only for an electron incident from the left. Following a transition, caused by a photon of energy  $\hbar\omega$ , from the transverse state  $(m, n)$  to the transverse state  $(m', n')$  at the generation point  $\tau$ , the electron encounters a higher barrier (with a maximum  $E_{m',n'}^{\max}$ ) which may backscatter the electron (see the dashed line indicating schematically the electronic trajectory).  $\gamma=1$  and  $\gamma'=-1$  denote transmitted and reflected modes, respectively.

that in the case of adiabatic separation of (transverse and longitudinal) variables in the Schrödinger equation, the transverse electronic energies in the microconstriction serve as scattering barriers for the longitudinal motion of the electrons<sup>6</sup> (see Fig. 1, where the mechanism of photon-induced indirect backscattering of electrons in a nanowire is depicted). One can therefore conclude that observation of the change in the conductance of a nanowire in the presence of irradiation would strongly support the concept of adiabatic quantum propagation in certain metallic and semimetallic nanowires. In this paper we will assume that such adiabatic classification of electronic states is valid, and show how photoconductance measurement may be used as a spectroscopy of such states. In our analysis we will consider microconstrictions characterized by a soft (harmonic) confining potential well. This model is likely to be most applicable to wires made of materials characterized by weaker screening, e.g., bismuth nanowires. Possible effects caused by anharmonic corrections to the confining potential are discussed.

In the following section we present a qualitative picture of microwave transport in 3D nanowires, with and without applied magnetic fields. A quantitative discussion of the proposed magneto-optical spectroscopy of electronic states in nanowires is given in Sec. III. We summarize and discuss our results in Sec. IV.

## II. QUALITATIVE PICTURE OF MICROWAVE-INDUCED TRANSPORT

We consider ballistic electronic transport through a 3D nanowire connecting two reservoirs. If a bias voltage  $V$  is applied to the system the equilibrium distributions in the left and right reservoirs are characterized by chemical potentials which differ by  $eV$ . For nanowires where the variation of the

cross section along the axis of the nanowire is adiabatic on the scale of the electron's wavelength, it is possible to separate variables corresponding to the transverse and longitudinal motion of the electron when solving the Schrödinger equation. Consequently, the quantized transverse motion can be described in terms of transverse energy levels  $[E_{m,n}(z)]$ , which are dependent on the longitudinal coordinate, and the longitudinal motion can be described as a one-dimensional (1D) propagation through the effective barrier set up by the transverse energy level occupied by the electron. Additionally, we consider our nanowire to be sufficiently long to allow neglect of tunneling effects on the electron's propagation. Under these conditions, states with the maximum value of their transverse energies (in the narrowest part of nanowire) higher than the electron's energy are reflected, while other electronic states are transmitted. We will denote a transmitted mode by  $|\alpha_{\rightarrow}\rangle$  and a reflected one by  $|\alpha_{\leftarrow}\rangle$ . Here  $\alpha \equiv (n, m, E_{\alpha})$  denotes the relevant quantum numbers. The photoconductance, i.e., the difference between the conductance of the nanowire in the presence of irradiation and the one without it, depends on the rate of transitions between transmitted and reflected states of the electron induced by the irradiation. These transitions, which may result in backscattering processes, give negative or positive net contributions to the current, depending on the relative position of the Fermi energy with respect to the middle between two nearest levels. We assume that the microwave field is polarized in the plane transverse with respect to the wire axis, such that the energy of the absorbed photon would go entirely into electronic transitions between the transverse energy levels, with no transfer of longitudinal momentum. Nevertheless, since it turns out that the longitudinal motion of the electron strongly depends on which transverse level it occupies, such a microwave-induced transition between transverse energy levels may drastically influence the propagation of the electron along the wire.

In Fig. 1 we sketch the effective 1D potential barriers for the longitudinal propagation of an electron occupying a transverse level characterized by the pair of quantum numbers  $(m, n)$ . A microwave-induced transition from the transverse level  $(m, n)$  to the level  $(m', n')$  implies that the electron will encounter now a different (higher) barrier which may eventually backscatter the electron. Consequently, a photon-induced transition between two quantized energy levels may block charge propagation through the channel. Because the level spacing depends on the position along the wire, the optical transition may take place only at special point(s)  $\tau$ , where resonant conditions are satisfied. We will refer to such points as generation points.

In order for the optical transition to take place the initial state of the electron should be occupied while the final state should be empty. In Fig. 2 we show the equilibrium distribution functions at zero temperature for the right [Fig. 2(a)] and left [Fig. 2(b)] reservoirs. We introduce the index  $\gamma$  to label transmitted ( $\gamma=1$ ) and reflected ( $\gamma=-1$ ) modes. For the left (right) reservoir, optical transitions between states with different  $\gamma$  make negative (positive) contribution to the current, while the transitions between states with the same  $\gamma$  do not change the current. One can easily see that the contributions to the current due to photon-induced transitions in the left and right reservoirs cancel each other except for tran-

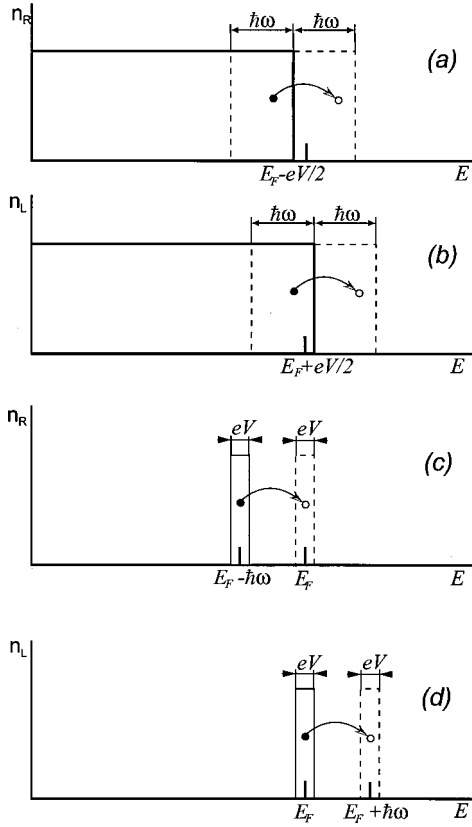


FIG. 2. Schematic equilibrium distribution functions at zero temperature for the right (a) and left (b) reservoirs; the short vertical marks in (a) and (b) denote the position of the Fermi energy  $E_F$ . Photon-induced transitions occur from the shaded areas and are schematically represented by arrows. The contributions to the current due to transitions between states incident from the left and right reservoirs cancel each other except for transitions from the  $eV$  vicinity of  $E_F - \hbar\omega$  between the states incident from the right reservoir [shaded area in (c)], and for the  $eV$  vicinity of  $E_F$  between the states incident from the left reservoir [shaded area in (d)].

sitions from the  $eV$  vicinity of  $E_F - \hbar\omega$  in the right reservoir [Fig. 2(c)] and for transitions from the  $eV$  vicinity of  $E_F$  in the left reservoir [Fig. 2(d)]. The first (second) type of transitions, which is allowed only in the right (left) reservoir, makes a positive (negative) contribution to the current.

In order to determine the transmission probability amplitudes between the electron's states we express the Hamiltonian as a sum of two terms:<sup>14</sup>

$$\hat{\mathcal{H}} = \hat{\mathcal{H}}_0 + \hat{\mathcal{H}}_{\text{int}}, \quad (1)$$

where  $\hat{\mathcal{H}}_0$  is the Hamiltonian in the absence of irradiation, and

$$\hat{\mathcal{H}}_{\text{int}} = \hat{V}_\omega \cos(\omega t), \quad \hat{V}_\omega = \frac{e\mathcal{E}_\omega}{m^*\omega} \hat{p}_y. \quad (2)$$

Here  $\mathcal{E}_\omega$  is the amplitude of the applied electromagnetic field which is assumed to be polarized in the (transverse)  $y$  direction (the  $z$  direction corresponds to the axis of the wire), and  $m^*$  is the effective mass of the electron. To first order in perturbation theory,<sup>12</sup> one obtains for the photoconductance

$$G^{\text{ph}}(\omega) = \frac{4\pi e^2}{\hbar} \sum_{\alpha, \beta} \frac{\partial f_\alpha^0}{\partial \mu} [|\langle \beta_- | \hat{V}_\omega | \alpha_- \rangle|^2 \delta(E_\alpha - E_\beta - \hbar\omega) - |\langle \alpha_- | \hat{V}_\omega | \beta_- \rangle|^2 \delta(E_\alpha - E_\beta + \hbar\omega)], \quad (3)$$

where  $\alpha$  is taken at the Fermi level, and  $f_\alpha^0$  is the Fermi-Dirac equilibrium electron distribution function. In Eq. (3) one can easily recognize the aforementioned two types of transitions in the left and right reservoirs.<sup>15</sup>

Let us consider the dependence of the photoconductance on the frequency of the photons,  $\omega$ . We will limit our discussion to the transition between the two electron states illustrated in Fig. 1. As we will see below, this limitation is justified in the framework of a parabolic confining potential model by the selection rules imposed by the matrix elements of the microwave field operator [see Eq. (3)]. In the absence of such selection rules optical transitions between several electronic states should be included; this makes quantitative analysis of the photoconductance more complicated, but yields qualitatively similar results as we discuss in Sec. IV. As we noted earlier, only optical transitions between transmitted and reflected electron states (i.e.,  $\gamma\gamma' = -1$ ) contribute to the photocurrent.

For small values of  $\omega$  (i.e.,  $\omega < \omega_1$ ; see Fig. 1), transitions between states incident from both reservoirs contribute to the photocurrent, essentially canceling each other.<sup>13</sup> On the other hand, for  $\omega > \omega_1$ , where

$$\omega_1 = \frac{E_{m',n'}^{\text{max}} - E_F}{\hbar}, \quad (4)$$

an electron state with energy  $E_F + \hbar\omega$  is transmitted ( $\gamma\gamma' = 1$ ), and the transitions in the left reservoir do not contribute to the photocurrent.

For  $\omega > \omega_2$ , where

$$\omega_2 = \frac{E_F - E_{m,n}^{\text{max}}}{\hbar}, \quad (5)$$

an electron state with energy  $E_F - \hbar\omega$  is reflected ( $\gamma\gamma' = -1$ ), and the transitions in the right reservoir (as well as the ones in the left reservoir) do not contribute to the photocurrent, such that the photoconductance vanishes for  $\omega > \omega_2$ . For  $\omega_1 < \omega < \omega_2$  the photoconductance is maximal due to contributions of the transitions in the right reservoir, which are not balanced by those in the left one. This results in a steplike structure for the dependence  $G^{\text{ph}}$  on  $\omega$ , as shown schematically in Fig. 3(a).

In the above discussion of the qualitative behavior of the photoconductance as a function of  $\omega$ , we assumed that  $E_F$  is located closer to the maximum value of the upper level than to the one of the lower level (as shown in the Fig. 1), i.e.,  $E_{m',n'}^{\text{max}} - E_F < E_F - E_{m,n}^{\text{max}}$ , which determined the major contributions to the photocurrent of the transitions in the right reservoir for  $\omega_1 < \omega < \omega_2$ .

In the opposite case, when  $E_{m',n'}^{\text{max}} - E_F > E_F - E_{m,n}^{\text{max}}$ , (i.e., for  $\omega_2 < \omega_1$ ), one easily obtains a similar steplike dependence for  $G^{\text{ph}}(\omega)$ , where for  $\omega_2 < \omega < \omega_1$  only transitions in the left reservoir contribute to the photocurrent, resulting in a negative step in  $G^{\text{ph}}(\omega)$  [see Fig. 3(b)].

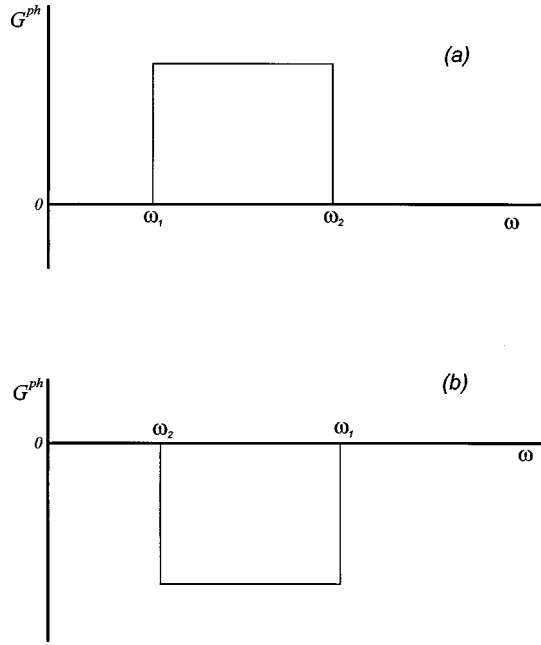


FIG. 3. Schematic description of the dependence of the photoconductance on the frequency of the microwave field  $\omega$ . The case of  $\omega_1 < \omega_2$  is shown in (a), where  $\omega_1$  and  $\omega_2$  are defined by Eqs. (4) and (5), respectively (see also Fig. 1). Transitions with  $\omega < \omega_1$  between states incident from both reservoirs contribute to the photoconductance, canceling each other and resulting in zero photoconductance. For  $\omega_1 < \omega < \omega_2$ , transitions between states incident from the left reservoir do not contribute to the photocurrent, and the total photoconductance is maximal. Finally, for  $\omega > \omega_2$  transitions between the states incident from both reservoirs do not contribute to the photocurrent, resulting in zero photoconductance. An analogous steplike dependence (with negative steps) occurs for the case of  $\omega_1 > \omega_2$  shown in (b).

Determination of the critical frequencies  $\omega_1$  and  $\omega_2$  may provide important information about the electronic energy levels in the constriction. For example, from Eqs. (4) and (5), it follows that

$$E_{m',n'}^{\max} - E_{m,n}^{\max} = \hbar\omega_2 + \hbar\omega_1 \quad (6)$$

and

$$E_F - \frac{1}{2}(E_{m',n'}^{\max} + E_{m,n}^{\max}) = \frac{1}{2}(\hbar\omega_2 - \hbar\omega_1). \quad (7)$$

Expression (6) allows us to evaluate the level spacing in the bottleneck of the constriction. This allows us to estimate the effective size of the narrowest part of the nanowire, e.g., for a parabolic confining potential  $E_{m',n'}^{\max} - E_{m,n}^{\max} = \hbar\omega_0^{\max}$ , where  $\omega_0^{\max}$  is the characteristic parameter of the parabolic confining potential in the narrowest part of the constriction. Furthermore, expression (7) allows one to estimate the position of the electron Fermi energy in the constriction relative to the middle point between two neighboring energy levels.

Additional spectroscopic information can be obtained if a static magnetic field is applied along the nanowire. In the presence of a longitudinal magnetic field ( $H$ ) the transverse energy level spectrum in a parabolic confining potential is given by

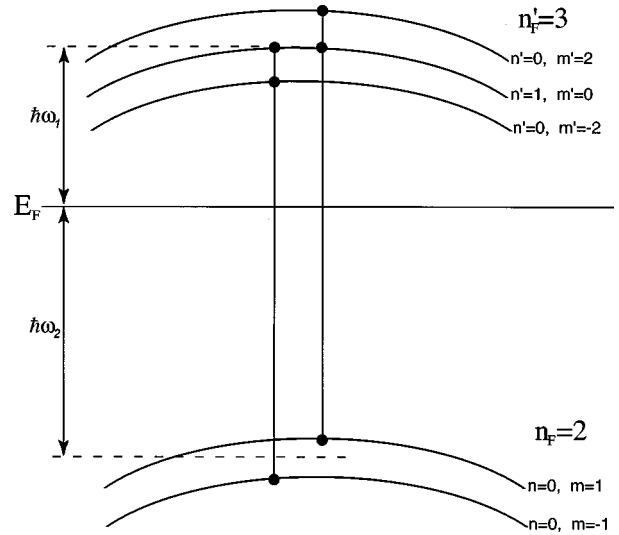


FIG. 4. Splitting of the transverse energy levels in a longitudinal magnetic field. Allowed transitions (due to selection rules imposed by the parabolic confining potential, i.e.,  $\Delta n = 0, 1$ , and  $\Delta m = \pm 1$ ) between the transverse energy levels characterized by the numbers  $n_F$  and  $n'_F = n_F + 1$  are denoted by vertical lines. Comparison with the magnetic-field-free case displayed in Fig. 1 shows that under the influence of a longitudinal magnetic field the critical frequency  $\omega_1$  is split  $n'_F$  times, and the frequency  $\omega_2$  is split  $n_F$  times.

$$E_{mn}(z) = \hbar[\omega_c^2/4 + \omega_0^2(z)]^{1/2}n_F + \frac{1}{2}m\hbar\omega_c, \quad (8)$$

where  $n_F = 2n + |m| + 1$ ,  $\omega_c = eH/m^*c$  is the cyclotron frequency, and  $\omega_0(z)$  is the frequency parameter characterizing the confining potential [see Eq. (9) below; also see Ref. 16]. In the absence of the magnetic field the transverse energy levels are degenerate, with the  $n_F$ th level being  $n_F$ -fold degenerate. In a weak magnetic field ( $\omega_c \ll \omega_0$ ) this degeneracy is removed, and the transverse energy levels are split into sublevels with spacings of  $\hbar\omega_c$  (see Fig. 4). Due to the selection rules in a parabolic potential (described in Sec. III), only transitions with  $\Delta n = 0, 1$  and  $\Delta m = \pm 1$  are allowed. Consequently, for any given split level, characterized by the index  $n_F$ , there are only two allowed transitions to the level  $n'_F = n_F + 1$  (see Fig. 4). Now we can repeat our discussion of the dependence of  $G^{\text{ph}}(\omega)$  on the photon frequency  $\omega$ , taking into account the splitting of transverse energy levels due to presence of the magnetic field. It is easily observed (Fig. 4) that the frequency  $\omega$  for which upper ( $n'_F$ ) levels become transmitted modes is now different for each level; i.e., the critical frequency  $\omega_1$  discussed above is now split  $n'_F$  times. Similarly, the frequency  $\omega_2$  is split  $n_F$  times. This splitting results in the appearance of microsteps in  $G^{\text{ph}}$  as a function of the photon frequency  $\omega$  (see Fig. 5). The number of microsteps corresponding to the splitting of the critical frequency  $\omega_1$  (“ascending” microsteps) is equal to  $n'_F$ , while the number of microsteps corresponding to the splitting of the critical frequency  $\omega_2$  (“descending” microsteps) is equal to  $n_F$ ; i.e., for a parabolic confining potential the difference between the numbers of “ascending” and “descending” microsteps should be equal to 1. This result may be used to assess “the softness” of the confining potential as we discuss in Sec. IV. Furthermore, from the observation of the microstructure in the dependence of  $G^{\text{ph}}$  on  $\omega$  one may ob-

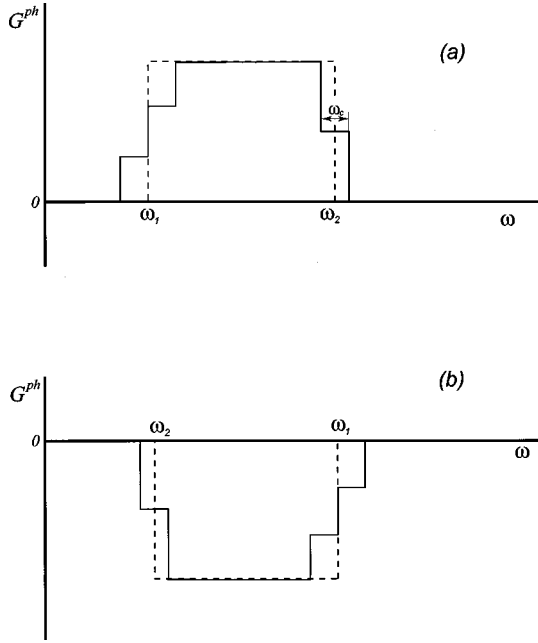


FIG. 5. Schematic dependence of the photoconductance on the frequency of the microwave field  $\omega$  in the presence of a longitudinal magnetic field for  $\omega_1 < \omega_2$  (a) and  $\omega_1 > \omega_2$  (b). The critical frequencies  $\omega_1$  and  $\omega_2$  are split  $n_F + 1$  and  $n_F$  times, respectively (compare to Fig. 4), resulting in the appearance of microsteps in the dependence of the photoconductance on  $\omega$ . The number of ascending microsteps corresponds to the splitting of the critical frequency  $\omega_1$  and equals to  $n'_F = n_F + 1$ , while the number of descending microsteps corresponds to the splitting of the critical frequency  $\omega_2$  and is equal to  $n_F$ . The width of the microsteps corresponds to the cyclotron frequency  $\omega_c$  and can be used to determine the electrons' effective mass in the constriction.

tain  $n_F$ , which allows one to estimate the Fermi energy in the constriction. Additionally, the width of the microsteps corresponds to  $\omega_c$ , and hence it could be used to determine the effective mass ( $m^*$ ) of the electrons in nanowire. In Sec. III we formulate a quantitative approach for the magneto-optical spectroscopy of nanowires which we described above.

### III. MAGNETO-OPTICAL SPECTROSCOPY OF ELECTRONIC STATES IN NANOCONSTRICTIONS

#### A. Formulation of the problem

We consider ballistic electronic transport through a 3D constriction with a cylindrical symmetry, modeled by a harmonic confining potential

$$\Phi(\rho, z) = \Phi_0 + \frac{1}{2} m^* \omega_0^2(z) \rho^2. \quad (9)$$

Here  $z$  is the coordinate along the constriction axis,  $\rho$  is the radial (transverse) distance from the constriction axis, and  $m^*$  is the effective mass of the electron. The geometry of the potential (effective length of the constriction) is determined by the confining frequency  $\omega_0(z)$ . In order to neglect the photocurrent in the absence of a driving voltage [see Eqs. (1) and (2)], we will assume that the microconstriction is symmetrical with respect to the plane containing the minimal (at  $z = 0$ ) cross section, i.e.,  $\omega_0(z)$  is taken to be an even function of  $z$ . We will also assume that this function varies slowly on the scale of the electron Fermi wavelength to ensure adiabaticity of the electron propagation through the wire.

To calculate the photoconductance<sup>10</sup> we have to evaluate the matrix element  $V_{\alpha\beta} \equiv |\langle \alpha_- | \hat{V}_\omega | \beta_- \rangle|$  [see Eq. (3)]. We analyze the electronic transport through the constriction in the presence of a longitudinal ( $H \parallel \hat{z}$ ) magnetic field. In this case, with the symmetric gauge of the vector potential  $\vec{A} = \frac{1}{2}(-Hy, Hx, 0)$ , the unperturbed part of the Hamiltonian [see Eq. (1)] is given by

$$\hat{\mathcal{H}}_0 = \frac{1}{2m^*} \left( \vec{\mathbf{p}} - \frac{e}{c} \vec{A} \right)^2 + \Phi(\rho, z). \quad (10)$$

The slow variation of the function  $\omega_0(z)$  describing the (axial) shape of the constriction allows us to use the adiabatic method of separation of transverse and longitudinal variables, and the wave function can be written in the form

$$\Psi(\rho, \varphi, z) = \chi_z^{mn}(\rho, \varphi) Z(z). \quad (11)$$

Here  $\chi_z^{mn}(\rho, \varphi)$  is the transverse part of the wave function which can be expressed in terms of the confluent hypergeometric function  $F$ ,

$$\chi_z^{mn}(\rho, \varphi) = \frac{e^{im\varphi}}{\sqrt{2\pi}} \frac{1}{a^{1+|m|}} \left( \frac{(|m|+n)!}{2^{|m|} n!} \right)^{1/2} \frac{1}{|m|!} \times e^{-(\rho^2/4a^2)} \rho^{|m|} F\left(-n, |m|+1, \frac{\rho^2}{2a^2}\right), \quad (12)$$

where  $a = \sqrt{\hbar/m^* \omega^*}$ , and  $\omega^*(z) = \sqrt{\omega_c^2 + 4\omega_0^2(z)}$ ,  $n = 0, 1, 2, \dots$ , and  $m = 0, \pm 1, \pm 2, \dots$ . The spectrum of the transverse eigenvalues, given by Eq. (8), is a straightforward generalization of the Fock-Darwin spectrum<sup>17</sup> to an adiabatically varying confinement characterized by a frequency  $\omega_0(z)$  [see Eq. (9)]. Calculation of the matrix element between the transverse parts of the wave functions yields

$$|\langle \chi_z^{mn}(\rho, \varphi) | \hat{V}_\omega | \chi_z^{m'n'}(\rho, \varphi) \rangle|^2 = \frac{\hbar \omega^* e^2 \mathcal{E}_\omega^2}{8m^* \omega^2} S(m, n, m', n'), \quad (13a)$$

where

$$S(m, n, m', n') = \delta_{m, m'-1} \{ \theta(m') [(m' + n') \delta_{n, n'} + (n' + 1) \delta_{n, n'+1}] + \theta(-m' + 1) [ (|m'| + n' + 1) \delta_{n, n'} + n' \delta_{n, n'-1} ] \} + \delta_{m, m'+1} \{ \theta(-m') [ (|m'| + n') \delta_{n, n'} + (n' + 1) \delta_{n, n'+1} ] + \theta(m' + 1) [ (m' + n' + 1) \delta_{n, n'} + n' \delta_{n, n'-1} ] \}, \quad (13b)$$

and  $\theta(x)$  is the Heaviside step function, i.e.,  $\theta(x)=1$  for  $x > 0$  and  $\theta(x)=0$  otherwise.

The longitudinal wave functions for the transmitted [Eq. (14)] and reflected [Eq. (15)] modes are taken as

$$Z_{\alpha-}(z) = \left( \frac{m^*}{2\pi\hbar^2 k_\alpha(z)} \right)^{1/2} \exp\left( i \int^z k_\alpha(z') dz' \right) \quad (14)$$

and

$$Z_{\beta-}(z) = \left( \frac{2m^*}{\pi\hbar^2 k_\beta(z)} \right)^{1/2} \sin\left( \int_{z_r^\beta}^z k_\alpha(z') dz' + \frac{\pi}{4} \right), \quad (15)$$

with

$$k_\alpha(z) = \sqrt{2m^*[E_\alpha - E_{mn}(z)]/\hbar^2} \quad (16)$$

and similarly for  $k_\beta(z)$  with  $E_\alpha$  replaced by  $E_\beta$ . The point  $z_r^\beta$  on the axis of the wire denotes the classical turning point.

When evaluating the matrix element between the longitudinal parts of the wave functions we use the stationary phase approximation. The stationary phase point  $\tau$  (the generation point, see Sec. II and Fig. 1) is the point where the photon-induced transition occurs and the longitudinal momentum is conserved,<sup>10</sup> i.e.,  $k_\alpha(\tau) = k_\beta(\tau)$ . The part of the matrix element between the longitudinal components of the wave functions is given by

$$|\langle Z_\alpha(z) | Z_\beta(z) \rangle|^2 = \left| \frac{m^* \omega^*(\tau)}{4\pi\hbar^3 k_\alpha(\tau) \omega_0(\tau) \omega'_0(\tau) D_{m',n'}^{m,n}} \right|, \quad (17)$$

where  $D_{m',n'}^{m,n} \equiv 2(n' - n) + |m'| - |m|$ , and  $\omega'_0(\tau)$  denotes the derivative of  $\omega_0(z)$  with respect to  $z$  evaluated at the generation point  $z = \tau$ .

As a concrete example, we take for  $\omega_0(z)$  an exponential form

$$\omega_0(z) = \omega_0^{\max} \exp\left( -\frac{z^2}{2L^2} \right), \quad (18)$$

where  $L$  is the effective length of the constriction. For convenience we introduce several dimensionless parameters

$$\Omega_H = \frac{\hbar \omega_c}{E_F}, \quad \Omega_R = \frac{\hbar \omega}{E_F}, \quad s = \frac{E_F}{\hbar \omega_0^{\max}}. \quad (19)$$

Here  $s$  has the meaning of  $k_F r_0/2$  where  $r_0$  is the effective radius of the constriction for an electron at the Fermi level. The parameters  $\Omega_H$  and  $\Omega_R$  characterize the strength of the magnetic field and the energy of the photons, respectively.

For the chosen geometry of the constriction [Eq. (18)] one easily finds for the generation points

$$\tau = \pm L \sqrt{-2 \ln(s) - \ln\left\{ [(\Omega_R - \Omega_H(m' - m)/2)/D_{m',n'}^{m,n}]^2 - \Omega_H^2/4 \right\}}. \quad (20)$$

For the sake of convenience [see Eq. (23) below], we introduce a couple of auxiliary quantities

$$k_{\alpha,s} = k_F \sqrt{1 + s - [2\Omega_R - \Omega_H(m' - m)](n' + |m'|/2 + 1/2)/D_{m',n'}^{m,n} - \Omega_H m'/2} \quad (21)$$

and

$$\begin{aligned} \xi_s \left( \begin{matrix} m, n \\ m', n' \end{matrix} \right) &= \frac{1}{k_{\alpha,s}} \left\{ \theta[1 + s - \Omega_R - \sqrt{\Omega_H^2 + 4/s^2}(n + |m|/2 + 1/2) - \Omega_H m/2] \right. \\ &\quad \left. \times \theta[\sqrt{\Omega_H^2 + 4/s^2}(n' + |m'|/2 + 1/2) + \Omega_H m'/2 - s - 1] \right\}, \end{aligned} \quad (22)$$

where  $s=0$  or  $\Omega_R$ .

When the electronic state characterized by the quantum numbers  $n'$  and  $m'$  corresponds to the Fermi energy  $E_F$ , then the longitudinal wave-vector at the generation point  $z = \tau$  is given by Eq. (21) with  $s=0$ , and when that electronic state corresponds to the energy  $E_F + \hbar\omega$  then the longitudinal wave vector at the generation point  $\tau$  is given by Eq. (21) with  $s = \Omega_R$ . In Eq. (22) the product of the step functions for  $s=0$  ensures that the state characterized by the energy  $E_F - \hbar\omega$  and quantum numbers  $n$  and  $m$  is a transmitted one while the state with energy  $E_F$  and quantum numbers  $n'$  and  $m'$  is not. Similarly, for  $s = \Omega_R$ , Eq. (22) ensures that the state with energy  $E_F$  and quantum numbers  $n$  and  $m$  is a transmitted one while the state with  $E_F + \hbar\omega$ ,  $n'$ , and  $m'$  is not.

Combining the above expressions the photoconductance can be written as

$$\begin{aligned} G^{\text{ph}}(s) &= \frac{2e^2}{h} \left( \frac{e\mathcal{E}_\omega}{\hbar\omega} \right)^2 \frac{L^2 \pi}{8} \sum_{\substack{m,n \\ m',n'}} \frac{\left[ 4 + \Omega_H^2 s^2 \exp\left( \frac{\tau^2}{L^2} \right) \right]}{|\tau D_{m',n'}^{m,n}|} \\ &\quad \times S(m, n, m', n') \left[ \xi_0 \left( \begin{matrix} m, n \\ m', n' \end{matrix} \right) - \xi_{\Omega_R} \left( \begin{matrix} m, n \\ m', n' \end{matrix} \right) \right]. \end{aligned} \quad (23)$$

## B. Results and discussion

Using the expression derived for the photoconductance in nanowires [Eq. (23)] we analyzed it quantitatively for various conditions. In Fig. 6 we display the dependence of the photoconductance on the dimensionless frequency  $\Omega_R$  of the microwave field for zero temperature and in the absence of a

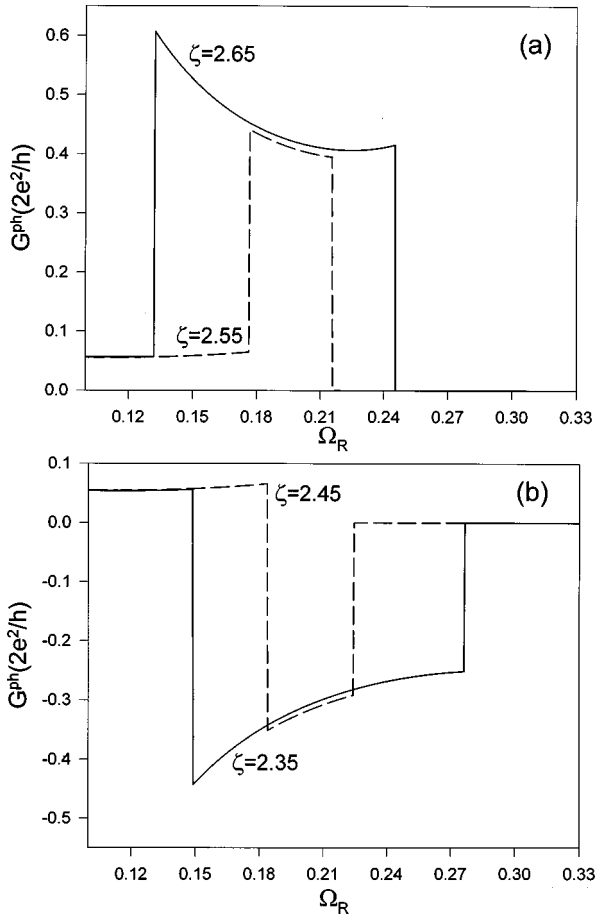


FIG. 6. Photoconductance (in units of  $2e^2/h$ ) plotted vs  $\Omega_R \equiv \hbar\omega/E_F$  for zero temperature and no magnetic field. In our calculations we used  $k_F = 2 \times 10^6 \text{ cm}^{-1}$ ,  $m^* = 0.1m_e$  (bismuth), an amplitude of the microwave field  $\mathcal{E}_\omega = 140 \text{ V/cm}$ , and an effective length of the constriction  $L = 3 \times 10^{-5} \text{ cm}$ . Values of the parameter  $\varsigma = E_F/\hbar\omega_0^{\text{max}}$  are indicated in the figure. In (a), the values of  $\varsigma$  (2.55 and 2.65) were chosen such that the Fermi level is closer to the upper transverse energy level in the narrowest part of the constriction, while in (b) the values of  $\varsigma$  (2.45 and 2.35) correspond to the Fermi level lying closer to the lower transverse energy level in the bottleneck of the constriction. Note the steplike behavior of the photoconductance as a function of  $\Omega_R$ .

magnetic field. In Fig. 6(a) the ratio of the Fermi energy of the electron to the maximum energy-level spacing (the parameter  $\varsigma$ ) was taken to be 2.65 and 2.55 (i.e., the Fermi energy is closer to the upper-energy level), while in Fig. 6(b) it was taken to be 2.35 and 2.45 (i.e., the Fermi energy is closer to the lower energy level). The qualitative picture discussed in Sec. II is portrayed in Fig. 6; that is, the photoconductance as a function of  $\Omega_R$  (or  $\omega$ ) has a well-pronounced steplike structure with two characteristic frequencies which, as discussed in Sec. II, can be used to determine the level spacing in the bottleneck of the constriction and the position of the Fermi energy with respect to the middle between two nearest levels. Note that the positions of the edge frequencies are related to the electronic parameters as discussed in connection with Eqs. (6) and (7). The precise behavior of  $G^{\text{ph}}(\Omega_R)$  is governed by the combination of matrix elements in Eq. (3), i.e., the nonzero photoconductance for small  $\Omega_R$  is due to incomplete compensation between the transitions with

positive and negative contributions to the photocurrent.<sup>13</sup> The behavior of  $G^{\text{ph}}(\Omega_R)$  for  $\omega_1 < \omega < \omega_2$  is determined by the matrix element for the transitions of electrons incident from the right reservoir. In the case when the Fermi energy is closer to the lower energy level the photoconductance step is negative [Fig. 6(b)], as was discussed earlier (compare to Fig. 3).

In Fig. 7 we display results for the photoconductance as a function of  $\Omega_R$  in the presence of an applied longitudinal magnetic field (compare to the qualitative picture given in Fig. 5). As aforementioned, the number of descending microsteps allows one to find  $n_F$ , and, thus to evaluate the absolute value of the Fermi energy in the constriction. The width of the microsteps corresponds to the cyclotron frequency  $\omega_c$  which allows evaluation of the electronic effective mass in the constriction (see Sec. II).

We note here that in both Figs. 6 and 7 the photoconductance at small (finite) values of  $\Omega_R$  [ $= \hbar\omega/E_F$ ; see Eq. (19)] is positive. To explain this behavior we observe from Eq. (3) that a transition from a state with energy  $E_F - \hbar\omega$  to a state with energy  $E_F$  makes a positive contribution to the current, while a transition from a state with energy  $E_F$  to one with an energy  $E_F + \hbar\omega$  results in a negative contribution to the current. Let us compare the matrix elements corresponding to these transitions for small values of  $\omega$  [i.e.,  $\omega < \omega_1$ ; see Eq. (4) for the definition of  $\omega_1$ ], where both types of transitions contribute to the current. For a given  $\omega$  the matrix elements between the transverse parts of the wave functions are the same for both types of photon-induced transitions [see Eqs. (13a) and (13b)], since they occur at the same generation point. The matrix element between the longitudinal components of the wave functions [see Eq. (17)] is inversely proportional to the longitudinal momentum (wave vector) at the generation point  $k_a(\tau)$  which follows from the normalization of the semiclassical longitudinal wave functions used in our model [Eqs. (14) and (15)]. It is easily seen (Fig. 1) that a transition from a state with energy  $E_F - \hbar\omega$  to the state with energy  $E_F$  corresponds to a smaller longitudinal momentum at the generation point than the transition from a state with energy  $E_F$  to a state with energy  $E_F + \hbar\omega$ . Consequently, the matrix element pertaining to the first type of transitions is larger than the one pertaining to the second type of transitions. Therefore for  $\omega < \omega_1$  positive contributions to the current prevail, resulting in a small positive photocurrent independent of the relative position of the Fermi energy with respect to the energy levels in the bottleneck of the constriction.

To illustrate the method of data analysis we will compute the ratio  $E_F/\hbar\omega_0^{\text{max}}$  [the parameter  $\varsigma$  in Eq. (19)] from the calculated photoconductance data, given in Figs. 6 and 7, and compare it to what was used as input to the calculations. From the data given by the solid line in Fig. 6(a), we determine that  $\Omega_1 \equiv \hbar\omega_1/E_F \approx 0.132$ , and  $\Omega_2 \equiv \hbar\omega_2/E_F \approx 0.245$ . Using Eq. (6) we obtain  $\Omega_1 + \Omega_2 = (E_{m',n'}^{\text{max}} - E_{m,n}^{\text{max}})/E_F = \hbar\omega_0/E_F = 1/\varsigma$ , i.e.,  $\varsigma = 1/(\Omega_1 + \Omega_2) = 1/0.377 \approx 2.65$ . Thus, analyzing the data (solid line) in Fig. 6(a) we recover the ratio  $E_F/\hbar\omega_0^{\text{max}} = \varsigma = 2.65$  used in the calculations that generated this data.

Let us now estimate the position of the Fermi energy with respect to the middle between the closest energy levels.

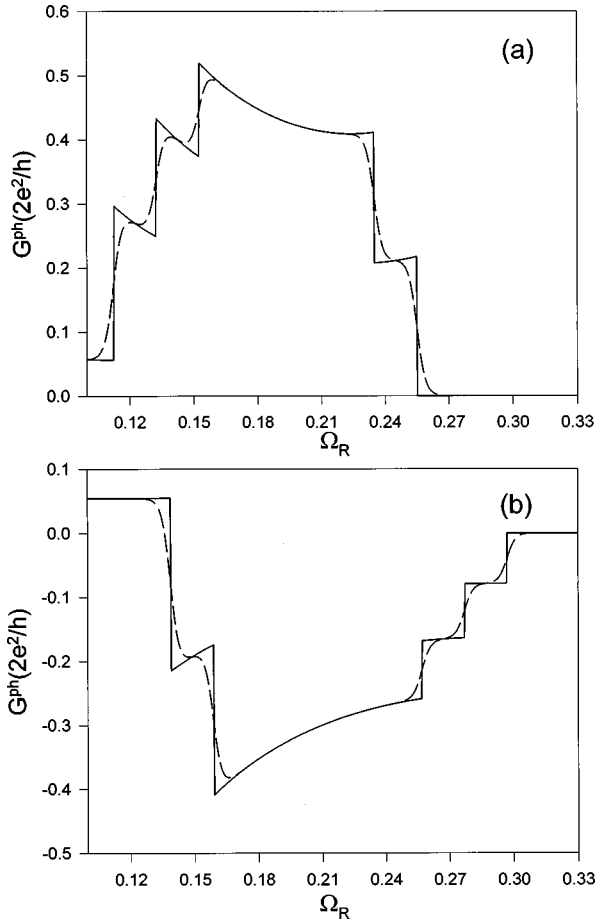


FIG. 7. Photoconductance (in the units of  $2e^2/h$ ) plotted vs  $\Omega_R$  in the presence of a longitudinal magnetic field. The strength of the magnetic field is characterized by the parameter  $\Omega_H \equiv \hbar \omega_c / E_F$ , which was taken to be 0.02. The solid lines correspond to the photoconductance at zero temperature, and the dashed lines correspond to the photoconductance at a temperature  $k_B T / E_F = 0.002$ . In (a),  $\xi = 2.65$ , and in (b)  $\xi = 2.35$ . The values of the parameters  $\mathcal{E}_\omega$ ,  $L$ , and  $k_F$  were taken to be the same as in Fig. 6.

From Eq. (7) we have  $[(E_{m',n'}^{\max} + E_{m,n}^{\max})/2 - E_F] / \hbar \omega_0^{\max} = (\Omega_2 - \Omega_1) E_F / 2 \hbar \omega_0^{\max} = \xi (\Omega_2 - \Omega_1) / 2$ , and from the data (solid line) in Fig. 6(a) we obtain  $[(E_{m',n'}^{\max} + E_{m,n}^{\max})/2 - E_F] / \hbar \omega_0^{\max} = 0.15$ . Thus, the ratio between the position of the Fermi energy with respect to the middle point between the closest energy levels, and the level spacing ( $\hbar \omega_0^{\max}$ ), is found to be 0.15 which corresponds to  $\xi = 2.65$  ( $\xi = 2.5$  corresponds to the Fermi energy being in the middle between two closest energy levels).

As a final illustration, we note that from the photoconductance in the presence of a magnetic field shown in Fig. 7, one can easily determine  $n_F = 2$  as the number of descending microsteps (compare to Figs. 4 and 5). Moreover, the width of microsteps ( $\hbar \omega_0 / E_F = 0.02$ ) allows one to determine the effective electron mass in the constriction.

#### IV. CONCLUSION

The analysis presented above shows that magneto-optical measurements on current carrying nanowires can in principle be used as a spectroscopic tool, enabling probing and detec-

tion of the quantum states of the electrons in a nanosize conductor. An important conclusion is that the very appearance of a regular structure in the dependence of the photocurrent on the photon frequency is a manifestation of the ballistic and adiabatic character of the electronic propagation in the nanowire, although we expect that such behavior will be maintained for circumstances where deviations from adiabatic character occur as long as they do not cause strong mode mixing. Moreover, we have demonstrated theoretically a method for determining from photoconductance measurements (with and without an applied magnetic field) important physical parameters of the system, such as the Fermi energy and effective mass of the electrons in nanowires, as well as the number of conducting modes.

The details of the spectroscopy discussed above were formulated for a harmonic confining potential, where the frequency dependence of the photoconductance is described by two characteristic frequencies  $\omega_1$  and  $\omega_2$  (see Figs. 3 and 4). The existence of only two characteristic frequencies originates from the fact that with a harmonic confinement potential only two electronic modes are involved in an optical transition affecting the photoconductance; this is a direct consequence of the selection rules for intermode transitions which are strictly valid only for a harmonic confining potential. Deviations from harmonicity would cause violation of these selection rules, resulting in the appearance of a complicated fine structure in the vicinity of the edges in  $G^{\text{ph}}(\omega)$ , which could complicate the spectroscopic analysis. However, for realistic potentials we believe that such a scenario is not the case, since calculations show<sup>18</sup> that for a hard-wall confining potential the additional optical transitions resulting from violation of the selection rules (compared to a soft potential) are characterized by matrix elements which are at least an order of magnitude smaller than the ones for transitions allowed by the selection rules. Therefore, we expect that the proposed spectroscopic probe would be a useful tool for realistic potentials, that is confinement potentials intermediate between the soft- and hard-wall confinement limits. One should expect the soft-wall confinement (or near-soft-wall confinement) used by us here to be valid particularly for systems with less efficient screening, e.g., semimetallic wires where the screening length is not as small as in ordinary metals. Moreover, our analysis (see Secs. II and III) suggests an independent check of the assumption that the confining potential is harmonic. The staircase in the  $G^{\text{ph}}(\omega)$  curve (Fig. 5), appearing in the vicinity of the edges at  $\omega_1$  and  $\omega_2$  in the presence of a longitudinal magnetic field, originates from magnetic-field-induced splitting of the degenerate electronic levels and the number of steps appearing near each edge is equal to the number of degenerate states corresponding to the two levels involved in the optical transition. Thus, experimental observations where those two numbers differ by 1, would correspond to a linear dependence of the level degeneracy on the level number, which is a direct manifestation of the harmonicity of the potential.

Another assumption which we made pertains to the axial symmetry of the nanowire, which was taken to have a cylindrical symmetry. Such an assumption seems to be natural for wires with nanosize cross sections where the surface energy makes an important contribution to the total energy of the wire. Small deviations from a cylindrical shape would result

in modifications of the transverse level degeneracies,<sup>4,19</sup> and in the appearance of a steplike structure in  $G^{\text{ph}}(\omega)$  even in the absence of a magnetic field. Our results, nevertheless, will be valid in this case for strong enough magnetic fields where field-induced splittings of energy-level degeneracies may exceed those caused by the geometrical anisotropy.

As aforementioned, the picture of photoconductance developed in this paper is based on an adiabatic approach, which implies negligible mode mixing. Usually this condition is valid for ballistic wires of adiabatic shapes. In our case one should formulate stronger conditions to prevent intermode relaxation of photoexcited, “hot” electrons; i.e., inelastic relaxations due to electron-electron and electron-phonon collisions may become operative and one should ensure that the length of the wire is smaller than the corresponding relaxation length. For 2D wires the corresponding criteria were formulated in Ref. 10. For our purposes, appropriate modifications need to be made to account for the three dimensionality of our system, as well as for the presence of a magnetic field. The latter circumstance implies that the typical frequency of electronic relaxations,  $\nu_{\text{inel}}$ , should be also smaller than the electronic level splitting in a magnetic field.

Electron-phonon relaxation appears to be inefficient for metallic nanowires with few conducting modes because the typical level spacing in microconstrictions (i.e., of the order of  $E_F$  divided by the number of modes) is larger than the Debye energy of the phonons  $\hbar\omega_D$ . For semimetals where  $E_F$  is of the order of  $\hbar\omega_D$  the corresponding momentum transfer (of the order of Fermi momentum of the electrons,  $p_F$ ) is much smaller than  $\hbar q_D$  and therefore the electron-phonon relaxation frequency,  $\nu_{e\text{-ph}}$ , becomes very small:  $\nu_{e\text{-ph}}/\omega_D \sim (\lambda_F q_D)^{-3}$ .<sup>20</sup>

Relaxation processes via electron-electron collisions may be the most important mechanism of electron relaxation in nanowires. The electron-electron collision frequency is proportional to<sup>21</sup>

$$\nu_{e-e} \sim \frac{1}{\hbar} \alpha^2 E_F \left( \frac{k_B T}{E_F} \right)^2, \quad (24)$$

where the interaction strength is characterized by the dimensionless parameter  $\alpha = e^2/\epsilon\hbar v_F$ , and  $\epsilon$  is the dielectric con-

stant (in Eq. 6.71 of Ref. 21,  $\epsilon \sim 1$  was taken). The factor  $(k_B T/E_F)^2$  originates from the Pauli principle. In our case  $k_B T$  may be replaced by the excitation energy of the electron (by the microwave field),  $\hbar\omega$ . Since the energy spacing between conducting modes is of the order of  $E_F$  divided by the number of modes, for nanowires with only a few conducting modes  $\hbar\omega \sim E_F$  and thus  $\nu_{e-e} \sim (1/\hbar)\alpha^2 E_F$ .

Consequently, in order for relaxation via electron-electron collisions to be ineffective we require that (i)  $L \ll l_{e-e}$  (where  $L$  is the length of the wire and  $l_{e-e}$  is the electron-electron mean free path), and (ii)  $\nu_{e-e} \ll \omega_c$ . Using the above expression for  $\nu_{e-e}$  we obtain, for criterion (i)

$$L \ll \lambda_F / \alpha^2. \quad (25a)$$

For a narrow wire with only a few conducting modes  $\lambda_F \sim r_0$ , where  $r_0$  is the radius of the wire. For criterion (ii) we may write

$$E_F \alpha^2 \ll \hbar\omega_c. \quad (25b)$$

From these conditions we observe that our analysis should apply for materials with a suppressed Coulomb interaction ( $\alpha < 1$ ). For metals  $v_F \approx 10^8$  cm/s and  $e^2/\hbar v_F \approx 1$ , and therefore the condition  $\alpha \ll 1$  can occur for  $\epsilon \gg 1$  (at a frequency of the order of  $E_F/\hbar$ ). Consequently, semimetallic wires are more promising for studies using the magneto-optical spectroscopy which we propose here. Taking parameters typical for bismuth [with a Fermi velocity  $v_F \approx 10^8$  cm/s and  $\epsilon \approx 10^2$  (Ref. 22)] one obtains  $\alpha \approx 10^{-2}$  and thus conditions (25a) and (25b) may be easily fulfilled for a bismuth nanowire with only a few modes (i.e., wires with cross-sectional radii of the order of several hundred Å).

#### ACKNOWLEDGMENTS

The research of S.B., L.Y.G., M.J., and R.I.S. was supported by the European ESPRIT project Nanowires, and the Swedish KVA and NFR. The research of A.G.S., E.N.B., and U.L. was supported by the U.S. Department of Energy, Grant No. FG05-86ER45234. Calculations were performed at the Georgia Tech Center for Computational Materials Science.

<sup>1</sup>U. Landman, W. D. Luedtke, N. Burnham, and R. J. Colton, *Science* **248**, 454 (1990).

<sup>2</sup>See reviews by U. Landman, W. D. Luedtke, and R. N. Barnett, in *Nanowires*, edited by P. A. Serena and N. Garcia (Kluwer, Dordrecht, 1997), pp. 109–132, and references therein; see also U. Landman, W. D. Luedtke, and J. Gao, *Langmuir* **12**, 4514 (1996).

<sup>3</sup>See articles and reviews in *Nanowires* (Ref. 2).

<sup>4</sup>E. N. Bogachek, A. M. Zagoskin, and I. O. Kulik, *Fiz. Nizk. Temp.* **16**, 1404 (1990) [*Sov. J. Low Temp. Phys.* **16**, 796 (1990)].

<sup>5</sup>B. J. van Wees, H. van Houten, C. W. J. Beenakker, J. G. Williamson, L. P. Kouwenhoven, D. van der Marel, and C. T. Foxon, *Phys. Rev. Lett.* **60**, 848 (1988); D. A. Wharam, T. J. Thornton, R. Newbury, M. Pepper, H. Ahmed, J. E. F. Frost, D. G. Hasko,

D. C. Peacock, D. A. Ritchie, and G. A. C. Jones, *J. Phys. C* **21**, L209 (1988).

<sup>6</sup>L. I. Glazman, G. B. Lesovik, D. E. Khmel'nitskii, and R. I. Shekhter, *Pis'ma Zh. Eksp. Teor. Fiz.* **48**, 218 (1988) [*JETP Lett.* **48**, 238 (1988)].

<sup>7</sup>R. N. Barnett and U. Landman, *Nature (London)* **387**, 788 (1997).

<sup>8</sup>See review by E. N. Bogachek, A. G. Scherbakov, and U. Landman, in *Nanowires* (Ref. 2), pp. 35–60.

<sup>9</sup>(a) E. N. Bogachek, A. G. Scherbakov, and U. Landman, *Phys. Rev. B* **56**, 14 917 (1997); (b) J. I. Pascual, J. A. Torres, and J. I. Saenz, *ibid.* **55**, R16 029 (1997).

<sup>10</sup>L. Y. Gorelik, M. Jonson, R. I. Shekhter, and O. Tegenan, in *Frontiers in Nanoscale Science of Micron/Submicron Devices*, Vol. 328 of *NATO Advanced Study Institute, Series E: Applied Sciences*, edited by A. Jauho and E. V. Bazaneva (Kluwer, Dordrecht, 1996), p. 225.

- <sup>11</sup>L. Y. Gorelik, A. Grincwajg, V. Z. Kleiner, R. I. Shekhter, and M. Jonson, *Phys. Rev. Lett.* **73**, 2260 (1994).
- <sup>12</sup>V. S. Borovikov, L. Y. Gorelik, V. Z. Kleiner, and R. I. Shekhter, *Low Temp. Phys.* **23**, 230 (1997).
- <sup>13</sup>L. Y. Gorelik, F. A. Maaø, R. I. Shekhter, and M. Jonson, *Phys. Rev. Lett.* **78**, 3169 (1997).
- <sup>14</sup>A. Grincwajg, L. Y. Gorelik, V. Z. Kleiner, and R. I. Shekhter, *Phys. Rev. B* **52**, 12 168 (1995).
- <sup>15</sup>The photocurrent for small values of  $\omega$  does not vanish completely because of the difference in the magnitudes of the matrix elements  $|\langle\beta_{-}|\hat{V}_{\omega}|\alpha_{-}\rangle|$  and  $|\langle\alpha_{-}|\hat{V}_{\omega}|\beta_{-}\rangle|$  in Eq. (3), as will be shown in the discussion of the numerical results. However these magnitudes are close, resulting in a very small photocurrent (photoconductance) for small  $\omega$ .
- <sup>16</sup>A. G. Scherbakov, E. N. Bogachek, and U. Landman, *Phys. Rev. B* **53**, 4054 (1996).
- <sup>17</sup>V. Fock, *Z. Phys.* **47**, 446 (1928); C. G. Darwin, *Proc. Cambridge Philos. Soc.* **27**, 86 (1930).
- <sup>18</sup>F. Geerinckx, F. M. Peeters, and J. T. Devreese, *J. Appl. Phys.* **68**, 3435 (1990).
- <sup>19</sup>E. N. Bogachek, A. G. Scherbakov, and U. Landman, *Phys. Rev. B* **56**, 1065 (1997).
- <sup>20</sup>A. A. Abrikosov, *Fundamentals of the Theory of Metals* (North-Holland, Amsterdam, 1988). In the discussion of electron-phonon relaxation rate (Chap. 4.3), the expression given in this reference [Eq. (4.20)] should include, on the right-hand side, the factor  $na^3$  (where  $n$  is the electron concentration and  $a$  is of the order of the lattice constant), which for typical metals is of the order of unity, while for semimetal it is much smaller. Consequently, Eq. (4.20) for  $k_B T \sim \hbar \omega_D$  yields for  $\nu_{e-ph}$  the expression given in the text.
- <sup>21</sup>R. E. Peierls, *Quantum Theory of Solids* (Oxford University Press, Oxford, 1965), Sec. 6.5.
- <sup>22</sup>W. S. Boyle and A. D. Brailsford, *Phys. Rev.* **120**, 1943 (1960); C. Nanney, *ibid.* **129**, 109 (1963).